Journal of Nuclear Materials 377 (2008) 378–384

Contents lists available at ScienceDirect

Journal of Nuclear Materials

journal homepage: www.elsevier.com/locate/jnucmat

Effect of flowing sodium on corrosion and tensile properties of AISI type 316LN stainless steel at 823 K

N. Sivai Bharasi [a,*], K. Thyagarajan [a], H. Shaikh [a], A.K. Balamurugan [b], Santanu Bera [d], S. Kalavathy [b], K. Gurumurthy [c], A.K. Tyagi [b], R.K. Dayal [a], K.K. Rajan [c], H.S. Khatak [a]

[a] Corrosion Science and Technology Division, Indira Gandhi Centre for Atomic Research, Kalpakkam 603 102, Tamil Nadu, India
[b] Materials Science Division, Indira Gandhi Centre for Atomic Research, Kalpakkam 603 102, Tamil Nadu, India
[c] Fast Reactor Technology Group, Indira Gandhi Centre for Atomic Research, Kalpakkam 603 102, Tamil Nadu, India
[d] Water and Steam Chemistry Division, Bhabha Atomic Research Centre, Kalpakkam 603 102, Tamil Nadu, India

ARTICLE INFO

Article history:
Received 15 February 2007
Accepted 31 January 2008

ABSTRACT

AISI type 316LN stainless steel was exposed to flowing sodium in mass transfer loop (MTL) at 823 K for 16 000 h and then examined for changes in the tensile properties due to the mass transfer and corrosion effects. Comparisons in microstructural and mechanical properties were made between annealed, thermally aged and sodium exposed materials. Microstructural examination of thermally aged and sodium exposed materials revealed precipitation of carbides at the grain boundaries. The sodium exposed samples contained a degraded layer at the surface up to a depth of around 10 μm and a surface carburized layer of about 30 μm. There was about 15% increase in yield strength and a decrease of about 20% in ductility for the sodium exposed material vis-a-vis thermally aged material and this was attributed to carburization effects and microstructural changes.

1. Introduction

Austenitic stainless steels of different grades are used as structural materials in primary circuit, IHX and piping in secondary loop of fast breeder reactors owing to their good compatibility with sodium in addition to their desirable properties of adequate high temperature mechanical properties and resistance to neutron irradiation. Sodium is used as coolant in liquid metal fast breeder reactors due to its multifaceted properties of high thermal conductivity, low vapour pressure, high boiling point, large heat capacity and low cost.

Long term exposure of austenitic stainless steels to high temperature sodium leads to mass transfer and corrosion. This corrosion is predominantly governed by the impurities present in the sodium, especially carbon and oxygen. Presence of oxygen in sodium significantly influences the corrosion processes [1,2] because leaching is usually preceded by the formation of ternary compounds of the steel constituents with oxygen and sodium. The most commonly encountered corrosion product in sodium containing less than 10 ppm oxygen is $NaCrO_2$ [3–5]. The transfer of elements from structural materials by liquid sodium is reported to influence the corrosion and mechanical properties [6–14].

It is well known that the behaviors of oxygen and carbon in sodium system have intimate relations with the corrosion behavior of steel. The chemical affinities of the elements with sodium differ. Oxygen forms a chemically stable oxide, Na_2O, which causes corrosion of steels; carbon forms a stable carbide, Na_2C_2, while nitrogen forms a chemically unstable nitride, Na_3N [15]. Solubility of oxygen is more than 1000 ppm at 500 °C [16] and that of C is about 30 ppm at 700 °C [17]. However, solubility of N is extremely small, far less than 1 ppb even at 700 °C [18].

Carbon is an important interstitial element and is required to impart strength to the stainless steel. Transport of carbon in the circuit due to difference in carbon activity in steels and sodium leads to carburization or decarburization, both of which have adverse effects on mechanical properties. Corrosion in sodium manifests through the following processes: (i) complete loss of material by leaching and consequent reduction in the wall thickness, (ii) preferential leaching of elements and generation of modified layer of inferior properties, (iii) formation of carburized or decarburized austenite layer, the depth of which depends on the duration of exposure, the temperature and carbon potential of sodium.

Most of the reports on influence of sodium on the mechanical properties pertain to tests carried out in sodium containing less than 5 ppm of carbon [12]. Indian sodium contains a total carbon content of approximately 25 ppm. To study the effects of sodium with such high concentration of carbon, a dynamic sodium loop simulating primary conditions of PFBR with respect to sodium velocity (5 m/s) and maximum temperature of 823 K, was

* Corresponding author.
E-mail address: sivai@igcar.gov.in (N. Sivai Bharasi).

0022-3115/$ - see front matter © 2008 Elsevier B.V. All rights reserved.
doi:10.1016/j.jnucmat.2008.01.032

constructed. In this loop, AISI type 316LN stainless steel samples were introduced and exposed for a time period of 16 000 h at the maximum temperature.

In PFBR, AISI type 316LN stainless steel, in which nitrogen is higher and carbon less as compared to conventional type 316 stainless steel was selected as construction material to counter the problem of sensitization and related aqueous corrosion issues during fabrication and storage. The changes in microstructure and tensile properties on exposure of type 316 stainless steel to flowing sodium at 823 K for 16 000 h have been investigated and reported [19]. In the present paper, changes in microstructure, carburization and their influence on the tensile properties of type 316LN stainless steel are discussed and compared with the results of type 316 stainless steel, the analysis of which was carried out earlier.

2. Experimental

2.1. Description of the loop

The dynamic mass transfer loop (MTL), was constructed using type 316 stainless steel. A schematic diagram is given in Fig. 1. The loop comprised of a main section and a purification section. The loop simulates the primary circuit of a reactor with respect to temperature, flow rate and material selection. The main loop consists of six test sections, three in the hot leg and three in the cold leg. Temperatures of the test sections were, 623, 723 and 823 K in the hot leg region and 723, 623 and 583 K in the cold leg region. The desired temperatures in these sections were attained by incorporating heaters and coolers between sample holders. Two electromagnetic pumps circulate sodium in the loop. The pumps generate the required flow rate and pressure. Velocity of the test sections was maintained at 5 ms^{-1} and flow rate in the main loop at 5.83×10^{-5} m^3 s^{-1}. The purification loop consists of a cold trap, a cold trap economiser, a plugging indicator, a plugging indicator economiser and a nickel tube sodium sampler. The functions of the cold trap and the plugging indicator were to control and monitor the impurity contents in sodium. Chemical composition of the 316LN stainless steel used for the studies is given in Table 1. Composition of the commercial grade sodium used in the loop is given in Table 2.

2.2. Description of the sample holder

The sample holders were made of type 316 stainless steel. They were cylindrical pipes of diameter 200 mm and length of 250 mm that were welded to the loop piping. Rectangular samples of type 316LN stainless steel with dimensions of 240 × 150 × 6 mm were kept in the sample holder. A 5 mm wide and 1 mm slit was cut on the surface of the plate through which sodium was allowed to flow at a velocity of 5 m/s. Only this part of the steel surface experiences sodium exposure, other areas just see only the temperatures. This was to facilitate delineation of thermal effects from corrosive effects by sodium. A schematic of the sample holder is shown in Fig. 2. After 16 000 h of sodium exposure at 823 K, the sample holder was cut from the loop, the samples were cleaned with methanol to remove the sticking sodium and subsequently washed with demineralised water. The specimens required for microstructural examination, microhardness measurements, sur-

Table 1
Chemical composition of type 316LN stainless steel

Element	C	N	Cr	Ni	Mo	Si	Mn	S	P	Fe
Composition (wt%)	0.03	0.085	16.0	11.2	2.0	0.60	1.3	0.005	0.042	Bal.

Table 2
Composition of commercial grade sodium used in the loop

Impurity element	O	C	Cl	Ca + Mg	Fe
Content, ppm	20	25	5	70	3

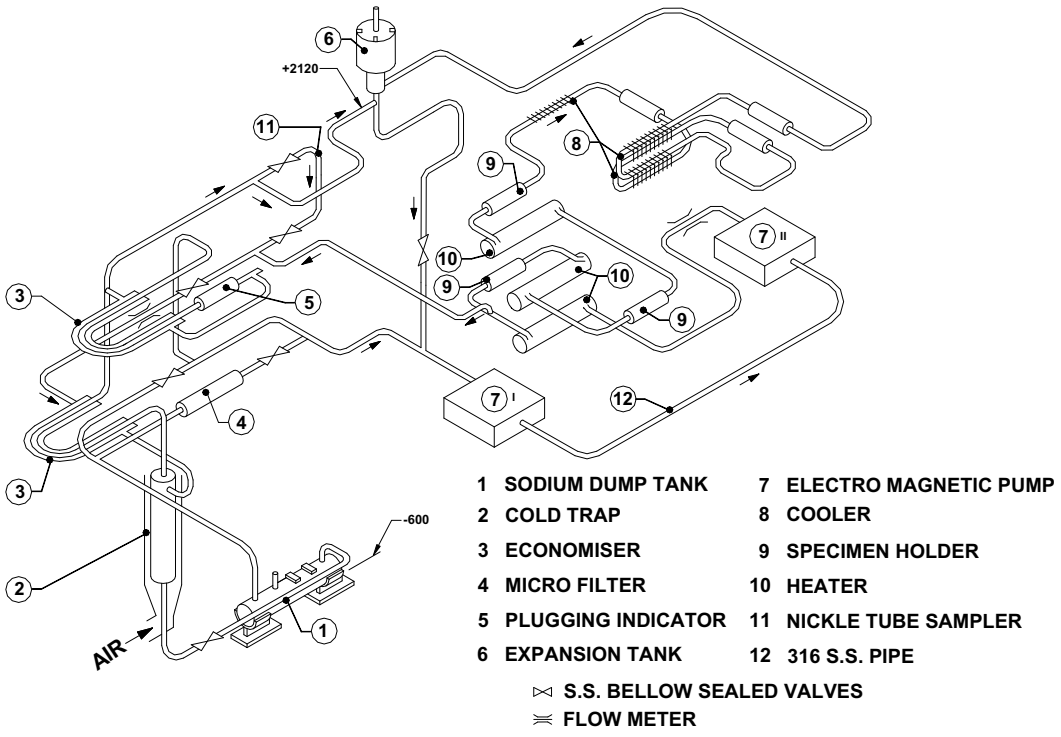

Fig. 1. Schematic of the mass transfer loop.

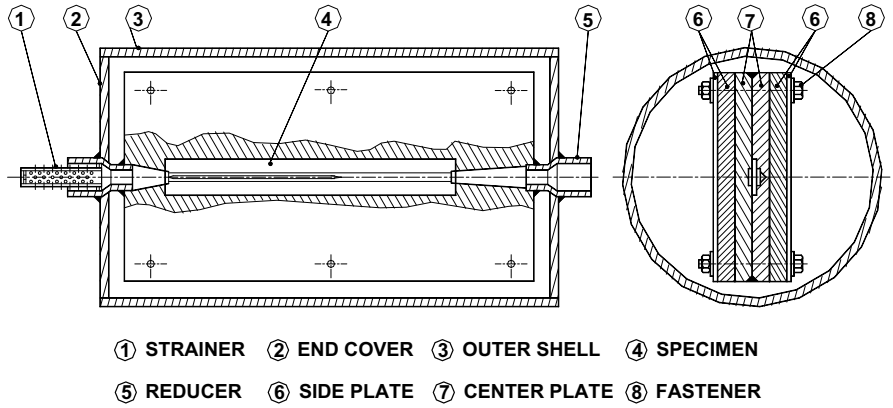

Fig. 2. Schematic of sample holder.

face analysis and tensile testing were prepared from these plates. Specimens were also prepared from mill-annealed type 316LN stainless steel for comparison studies with thermally aged and sodium exposed material.

2.3. Analysis of the sodium exposed specimens

AISI type 316LN stainless steel in the mill-annealed, thermally aged and sodium exposed condition were subjected to the following investigations.

2.3.1. Microstructural examination

Specimens were cross-sectionally mounted and polished to 1 μm surface finish by successively polishing with silicon carbide papers and diamond paste. The polished surface was then electrolytically etched in 10% ammonium persulphate solution. Microstructures were observed using optical and scanning electron microscopes.

2.3.2. Microhardness measurement

Specimens were mounted in cross-section and polished to mirror finish. Microhardness was measured using a Shimadzu make Model HMV-2 hardness tester under a load of 50 g. Hardness profile was obtained at periodic depth intervals from the surface.

2.3.3. X-Ray diffraction analysis

Phase changes generated due to leaching of elements by sodium from the surface of the steel were determined using a Stoe powder diffractometer in the GI XRD mode using Cu Kα radiation.

2.3.4. Analysis of corrosion product by XPS

The analyses of the corrosion products on sodium exposed surfaces were carried out using X-ray photoelectron spectrometer (XPS) in a ultra high vacuum (UHV) chamber at a pressure below 2×10^{-9} mbar. Al k-α (1486.6 eV) was used as the exciting source for the photoelectrons. The electrons were collected by a hemispherical analyzer of diameter 150 mm at 20 eV pass energy. The sodium exposed specimen was mounted inside the vacuum chamber of the XPS and the incident X-ray beam was directed on its surface. The energy of the photoelectrons emitted from the surface of the specimen was analyzed using a multichannel analyzer. From the energy spectrum of the emitted electrons, it was possible to determine the chemical state (oxidation state) of each element on the surface. Contamination on the surface of the specimen, due to handling, was removed by etching using an argon ion gun. The XPS spectrum was recorded after repeated etching to ensure that the effects of surface contamination were completely removed. The spectra of sodium, chromium, nickel, iron, oxygen, nitrogen and carbon were obtained separately to investigate the possibility of compound formation.

2.3.5. Carbon profile by secondary ion mass spectrometry

The changes in the concentration of carbon and elemental profiles of major alloying elements was obtained by using a secondary ion mass spectrometer (SIMS). The sodium exposed specimen was mounted with copper resin and polished up to 1 μm finish. Line scan analysis was carried out on the specimens which was mounted in cross-section. The primary ions employed were those of cesium of 3.3 keV energy. The beam size employed was 5 μm and analysis was carried at successive intervals from the surface. The intensities of the secondary ions of carbon were determined using a multichannel analyser.

2.3.6. Tensile test

Flat tensile specimens were machined from mill-annealed, thermally aged and sodium exposed samples. The sodium exposed region formed the gauge length of the tensile specimen. The tests were carried out in an INSTRON 1195 machine at an initial strain rate of $2.2 \times 10^{-4}\ s^{-1}$.

3. Results and discussion

Microstructural examination indicated a step structure for the mill-annealed material (Fig. 3(a)). A step structure occurs because of differences in the orientation of grains in the material. Thermally aged material revealed a structure with continuous precipitation of carbides at the grain boundaries (Fig. 3(b)). On etching in 10% by weight ammonium per sulphate solution, the carbides dissolve, giving rise to a ditch structure which shows up as thicker outlines at grain boundaries. The differences in the two structures influence the tensile properties of the stainless steel. In the case of the sodium exposed specimens, it was observed that, as in aged base metal, the carbides were distributed continuously along the grain boundaries. Carbide precipitation was also observed along twin boundaries in the austenite matrix. In addition to the ditch structure in sodium exposed specimens, where in width of ditch structure was greater at the surface than the bulk up to a depth of 30–40 μm, there was generation of a modified surface layer of less than 10 μm (Fig. 3(c) and (d)). This layer was similar to the one observed in sodium exposed 316 stainless steel [19]. However, the depth of degraded layer in type 316 stainless steel was around 15 μm. Analysis of this surface layer by XRD indicated the presence of ferrite phase (Fig. 4(a)). Fig. 4(b) shows the XRD pattern of the mill-annealed material which exhibits the highest intensity peak of austenite phase and absence ferrite phase. The formation of ferrite layer can be explained as follows: Exposure of stainless steel to

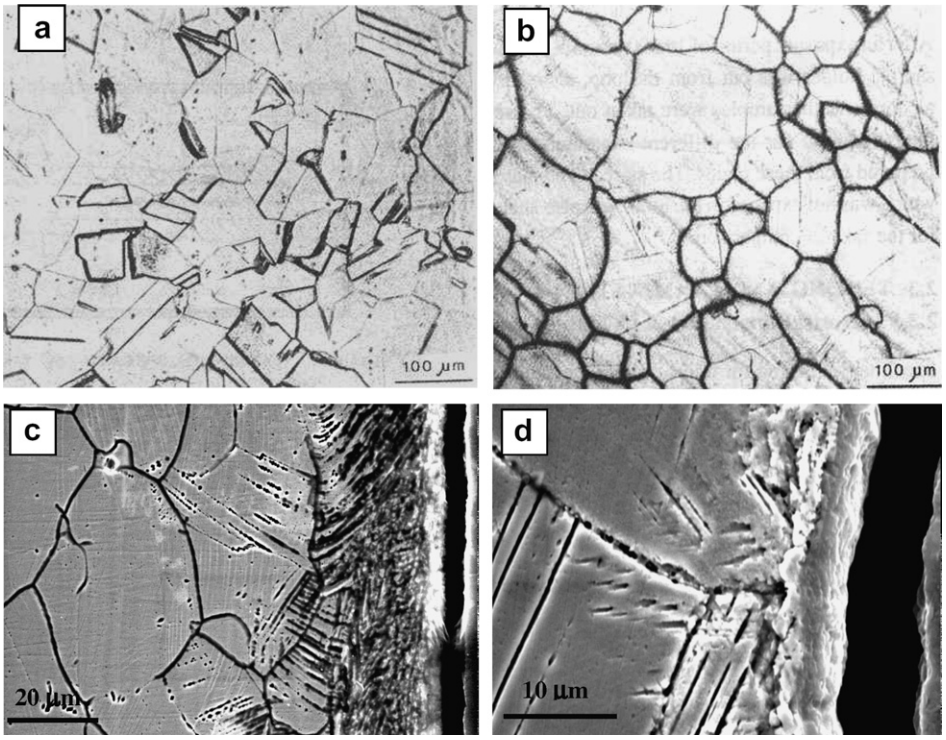

Fig. 3. Scanning electron micrographs of type 316LN stainless steel in (a) mill-annealed condition, (b) thermally aged condition, (c) and (d) different cross-sections of sodium exposed material showing surface carburization and ferrite layer, respectively.

high temperature sodium results in the dissolution of constituent elements into sodium [20,21]. Assisted by the temperature difference prevailing between different regions of the loop, the dissolved elements are transported to the cooler regions where they precipitate and deposit. The circulating sodium on reaching the higher temperature regions, dissolves additional quantities of the constituent elements and thus sustains the mass transfer process. This mode of transfer is a continuous process in a dynamic loop. Continuous leaching of elements such as nickel, chromium, molybdenum and manganese takes place. However, amongst the constituent elements of stainless steel, nickel possess the highest solubility in sodium, resulting in preferential leaching [20,21]. This leads to instability in the austenitic phase of the stainless steel and results in the formation of a ferrite layer in the microstructure. The other constituents of stainless steel do not show such leaching and deposition behaviour because of their relatively poor solubility in sodium. Moreover, the elements, iron, chromium and molybdenum form ternary compounds when adequate concentration of oxygen is available in sodium [22,23].

Rajendran Pillai et al. had reported that during exposure of type 316 stainless steel in sodium, at 823 K, resulted in significant depletion of nickel and chromium and a slight loss of molybdenum. The concentration of nickel at the surface was reduced to nearly 4 wt% compared with the 11.69 wt% originally present. Up to a depth of 10 μm from the surface the concentration of nickel was less than 5 wt%. Thereafter the concentration showed an increase and attained the matrix value at a depth of 15 μm. The concentration of chromium was in the range of 12–15 wt% up to a depth of 12 μm. The concentration attained the constant value of matrix at a distance of 25 μm. Observable leaching of molybdenum also occurred at this temperature and its concentration was less than 1 wt% up to a depth of 7 μm. At ~15 μm distance from the surface, the concentration attained that of the bulk matrix. In the present studies on type 316LN stainless steel, elemental leaching behaviour of Ni, Cr, Mo and Mn was investigated by the secondary ion mass spectroscopy technique (SIMS). It was found that the contents of Ni, Cr, Mo and Mn at a distance of about 0.35 μm from the surface was 7.5, 10.5, 1.4 and 0.41 wt% respectively. And these elements attained their matrix values at distances of 36, 25, 16 and 30 μm respectively (Fig. 5).

The average microhardness of the mill-annealed material was 174 VHN. The thermally aged samples showed an average hardness of 236 VHN. An increase of nearly 50 VHN was observed nearer the surface in sodium exposed material vis-a-vis thermally aged material (Fig. 6). The hardness values decreased and reached the matrix value at around 100 μm. This increase in hardness indicated surface carburization of the material due to sodium exposure. As seen Fig. 6, the thermally aged material showed uniform increase in hardness which was attributed to precipitation of carbides due to thermal effects.

Fig. 7 shows the XPS spectra of carbon, oxygen, chromium, iron, sodium and nitrogen obtained from the surface of sodium exposed sample. Very small signals could be detected from the spectrum of sodium indicating that trace amounts of sodium were present on the surface. Characteristic oxygen and carbon peaks were observed corresponding to their binding energies. The wide peak shape of O1s indicates that it is not present as single state. A narrow and sharp peak is characteristic of elemental oxygen. In general, the binding energy of 2p3/2 of elemental iron is 706.7 eV. In this case, the Fe 2p3/2 peak was observed at 710.5 eV. This chemical shift may be due to the formation of an iron compound with oxygen. In the figure, Cr2p3/2 is also presented where two peaks are marked by arrows. The lower energy peak corresponds to Cr–C and that the higher energy peak is due to the formation of Cr–O. The oxygen content in the sodium was probably below the threshold required for the formation of ternary compounds. Nitrogen enhancement on the surface was indicated by characteristic peak at around 400 eV. From the present analysis, it is not clear whether nitrogen is present in the elemental form or in the combined form. Even if present, that would be in trace amount as indicated by their

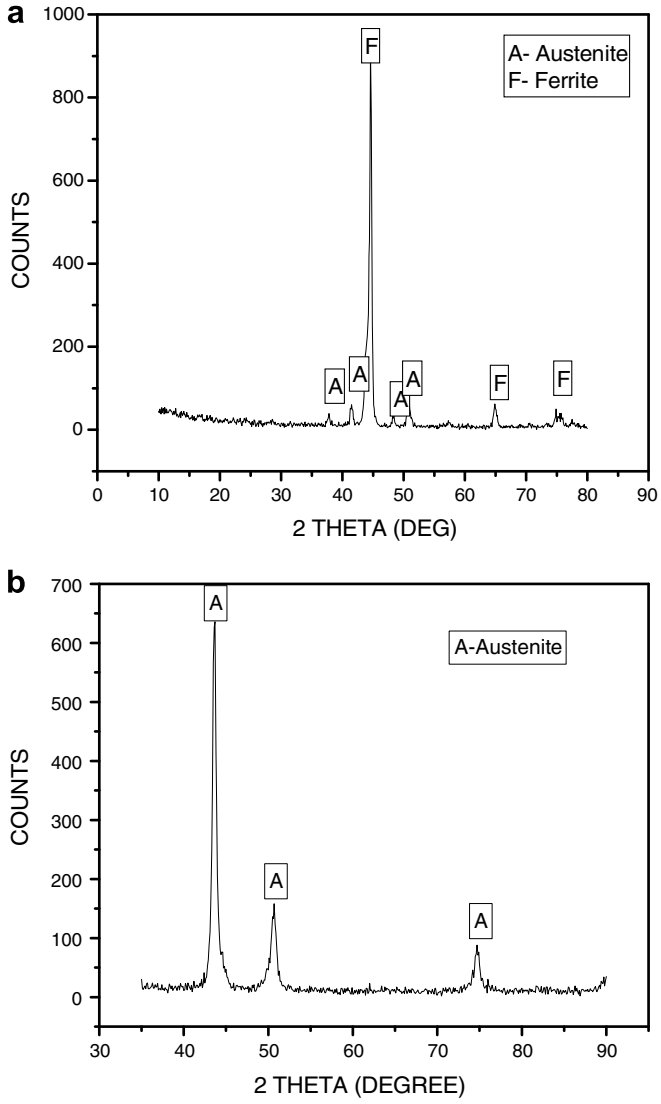

Fig. 4. X-Ray Diffraction pattern of (a) sodium exposed stainless steel and, (b) mill-annealed material.

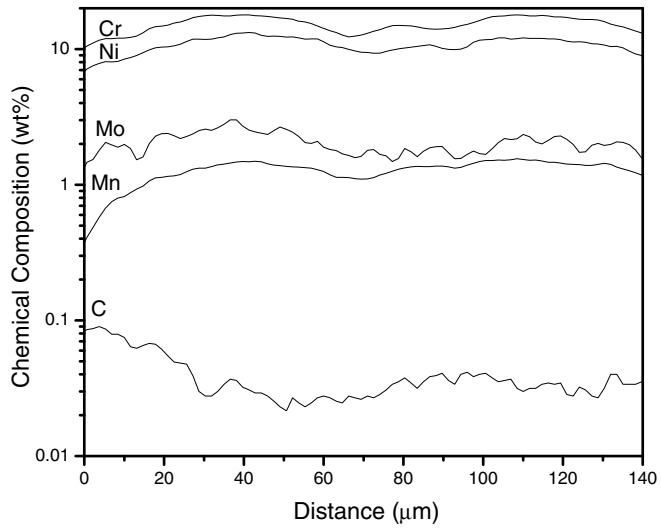

Fig. 5. SIMS profile of Cr, Ni, Mo, Mn and C of the sodium exposed sample.

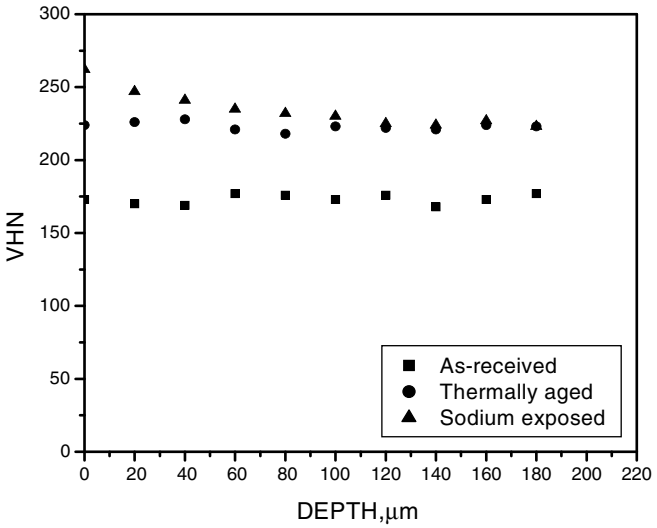

Fig. 6. Microhardness profile of the as received, thermally aged and sodium exposed material.

intensities. From the analyses of Fe 2p and Cr 2p, it is concluded that compounds containing Fe–O or Cr–O are formed on the surface of the specimen. Formation of ternary compounds could not be clearly established from the present studies or it is also possible that the compounds could have been washed out during the cleaning process. Investigation on type 316 stainless steel by XPS also did not indicate formation of ternary compounds.

The concentration profile of carbon determined by SIMS is shown in Fig. 8. As seen in the figure, the carbon concentration was maximum (0.09 wt%) at a depth of about 4 μm. The concentration thereafter reduced and reached the original concentration at a depth of 30 μm. Table 3 gives the surface carburization values as a function of distance for type 316 LN stainless steel exposed to sodium. In type 316 stainless steel, carbon concentration had attained a maximum of 0.135 wt% at a depth of 43 μm [14] and equaled the bulk concentration at a distance of 74 μm from the surface. In type 316LN stainless steel, the peak concentration of carbon was attained at 10 μm, immediately after the end of the degraded layer, while the bulk concentration was attained at a distance of 38 μm. The carbon content was less up to a depth where a degraded layer which contained ferrite was formed on the surface. The reduction in carbon content in the degraded layer was because the solubility of carbon in ferrite is lower resulting in carbon being rejected from the degraded layer. Comparative carbon profiles of type 316 and 316LN stainless steels, for the period of exposure of 16 000 h, measured by SIMS analysis is shown in Fig. 9. Based on the profile of carbon obtained by SIMS analysis, the effective diffusion coefficient (D_c^{eff}) of carbon in the stainless steel was calculated, the details of which are elaborated elsewhere [14]. The effective diffusion coefficient calculated was 7.85×10^{-18} m^2 s^{-1}. Using this value of D_c^{eff}, the expected carbon profile was determined for 40 years, which is shown in Fig. 10. In this calculation, it was assumed that the concentration of carbon had attained a dynamic equilibrium value of 0.09 wt% at the surface and it remained constant by further exposure to sodium. Such an assumption is valid because under the prevailing condition of low activity of carbon, the surface concentration is determined by carbon transfer by sodium and its diffusion in the material. The total carbon content in sodium is in large excess and the conversion of undissolved carbon into dissolved carbon facilitates the maintenance of near constant activity. The carburization profiles have been calculated after assuming a constant source of carbon in sodium. Ferrite layer is not taken into account in the calculation of diffusion coefficient and

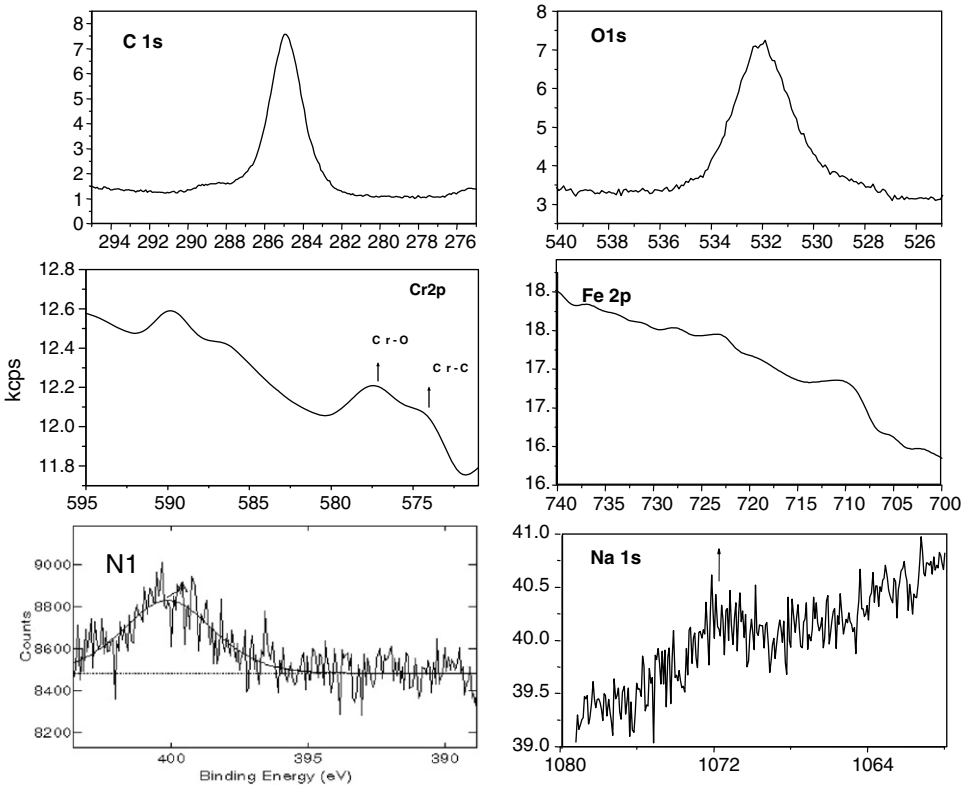

Fig. 7. XPS spectra of the carbon, oxygen, chromium, iron, nitrogen and sodium.

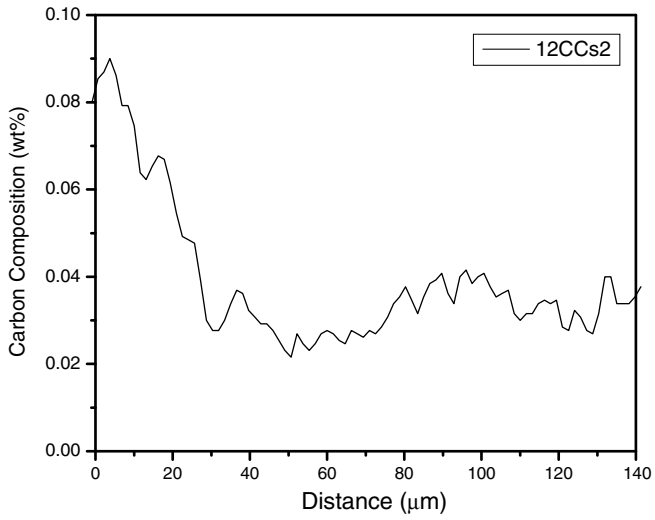

Fig. 8. Carbon profile of sodium exposed material from SIMS data.

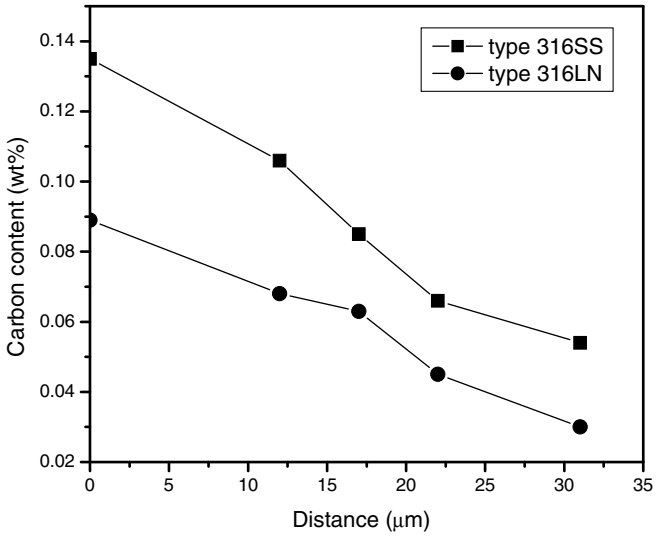

Fig. 9. Measured carbon concentration profile for types 316 and 316LN stainless steel exposed for 16 000 h obtained by SIMS analysis.

Table 3
Carbon concentration as a function of distance

Distance from the surface (μm)	Carbon content (wt%)
10	0.089
14	0.084
16	0.041
19	0.078
22	0.068
25	0.065
28	0.063
35	0.047
38	0.030

subsequent calculation of carbon profile, since concentration on the ferrite surface is lesser than the peak concentration on the austenite interface. The diffusion coefficient and subsequent calculation of carbon profile have been based on maximum carbon content measured by SIMS. Using the value of maximum carbon content would give a value of maximum carburized depth possible, which would then help in remnant life estimation. Also, the presence of carbides were not accounted for in the calculated carbon profiles since the size of the beam used in SIMS analysis was about 5 μm as against the carbide width of 2–4 μm. Hence, the effect of carbides on the calculated carbon profiles could not be delineated

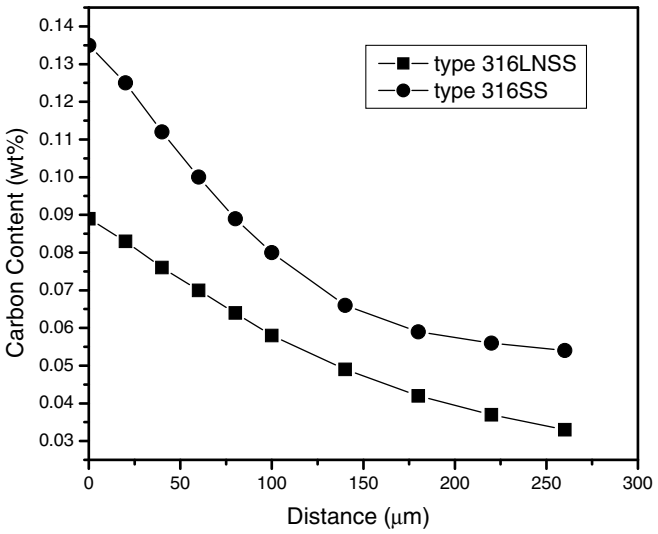

Fig. 10. Calculated carbon profiles of types 316 and 316LN stainless steel for 40 years.

Table 4
Tensile test results of type 316LN stainless steel exposed to sodium for 16000 h at 823 K

Material condition	YS (MPa)	UTS (MPa)	TE (%)
As-received	294	607	75
Thermally aged	319	653	65
Exposed to sodium	379	640	52

since the beam would cover both the particles and the matrix. Also, the presence of carbide would tie up the carbon thus making lesser amount of carbon available for diffusion to create carburized layers.

The room temperature tensile data of the specimens tested after 16000 h of sodium exposure is given in Table 4. No change in ultimate tensile strength (UTS) was observed between thermally aged and sodium exposed material. However, both these materials showed an increase in UTS vis-a-vis mill-annealed material. In the case of sodium exposed material, there was an increase of 15% in yield strength (YS) and reduction in ductility to 20% when compared to thermally aged specimens. This behaviour is attributed to the transport of carbon across the steel–sodium interface as is evident from SIMS analysis in Fig. 8. The increase in YS and reduction in ductility of the sodium exposed and thermally aged materials is attributed to hardening effect associated with the precipitation of carbides and also due to carburization in sodium. Due to thermal effect many transformations are brought about that affect the material properties [24]. Similar changes in mechanical properties were observed for type 316 stainless steel reported earlier [25].

4. Conclusions

AISI Type 316LN stainless steel was exposed to flowing sodium in a loop at a temperature of 823 K for 16000 h. The material was then analyzed to study the changes in microstructure and mechanical properties brought about by mass transfer. The main conclusions drawn from this investigation are as follows:

(1) Thermal ageing at 823 K caused carbide precipitation at the grain boundaries. Due to leaching of elements, there was a surface modified layer of ferrite up to around 10 μm.
(2) SIMS analysis indicated surface carburization up to 30 μm depth from the surface and the surface concentration was 0.09 wt% at 4 μm depth.
(3) Tensile test results showed that there was an increase of 15% in YS and a reduction in total elongation by 20% in sodium exposed material vis-a-vis thermally aged material which was attributed to carburization and carbide precipitation due to thermal ageing.
(4) From the measured carbon profiles by SIMS, effective diffusion coefficient was calculated and was used to predict the probable carbon profile for 40 years. The expected carburization depth was around 260 μm.
(5) Type 316LN stainless steel showed better resistance to mass transfer and carburization in high temperature flowing sodium than type 316 stainless steel.

References

[1] B.H. Kolster, J.V.D. Veer, L. Bos, in: H.U. Borgstedt (Ed.), Materials Behaviour and Physical Chemistry in Liquid Metal Systems, Plenum, New York, 1981, p. 37.
[2] M.G. Barker, D.J. Wood, J. Less Common Met. 35 (1974) 315.
[3] A.W. Thorley, A. Blundell, J.A. Bradley, in: H.U. Borgstedt (Ed.), Materials Behaviour and Physical Chemistry in Liquid Metal Systems, Plenum, New York, 1982, p. 5.
[4] S. Rajendran Pillai, H.S. Khatak, J.B. Gnanamoorthy, J. Nucl. Mater. 224 (1995) 17.
[5] T. Gnanasekaran, C.K. Mathews, J. Nucl. Mater. 140 (1986) 202.
[6] H. S. Khatak, Hasan Shaikh, J. B. Gnanamoorthy, in: Proceedings of the Fourth International Conference on Liquid Metal Engineering and Technology, vol. 2, European Nuclear Society, Avignon, France, 1988, 514-1.
[7] H.U. Borgstedt, G. Drechsler, G. Frees, H.S. Khatak, Z. Peric, B. Seith, J. Fracture 32 (1978) 155.
[8] G.J. Lloyd, Atomic Energy Rev. 16 (1978) 155.
[9] K. Natesan, O.K. Chopra, T.F. Kassner, J. Nucl. Mater. 73 (1977) 137.
[10] H. Huthman, G. Menken, H. U. Borgstedt, T. Tass, in: Proceedings of the Second International Conference on Liquid Metal Technology in Energy Production, J. M. Dahlke (Ed.), Richland, Washington, vol. 2, 1980, p. 19.
[11] K. Natesan, T.F. Kassner, Che Yu Li, Reactor Technol. 19 (1972) 244.
[12] J.L. Krankota, Eng. Mater. Technol. (1976) 9.
[13] H.S. Khatak, J.B. Gnanamoorthy, P. Rodriguez, R.D. Kale, K. Swaminathan, M. Rajan, K.K. Rajan, in: H.U. Borgstedt, G. Frees (Eds.), Liquid Metal Systems, Plenum, New York, 1995, p. 121.
[14] S. Rajendran Pillai, H.S. Khatak, N. Sivai Bharasi, A.K. Tyagi, J.B. Gnanamoorthy, R.D. Kale, Trans. Indian Inst. Met. 50 (1997) 103.
[15] R.J. Pulham, P. Hubberstey, J. Nucl. Mater. 115 (1983) 239.
[16] D. L. Smith, R. H. Lee, USAEC Report ANL-7891, 1972.
[17] R. Ainsley, L.P. Hartlib, P.M. Holroyd, G. Long, J. Nucl. Mater. 52 (1974) 255.
[18] H.U. Borgstedt, C.K. Mathews, Applied Chemistry of the Alkali Metals, Plenum Press, New York, London, 1987. p. 21.
[19] S. Rajendran Pillai, H.S. Khatak, J.B. Gnanamoorthy, S. Velmurugan, in: A.K. Tyagi, R.D. Kale, K. Swaminathan, M. Rajan, K.K. Rajan (Eds.), Mater. Sci. Technol. 13 (1997) 937.
[20] T.D. Claar, Reactor Technol. 13 (1970) 124.
[21] S. P. Awasthi, H. U. Borgstedt, PSB Ber. 1514(K1.II), Kemforschungszentrum, Karlsruhe, 1981.
[22] A.M. Azad, O.M. Sreedharan, J.B. Gnanamoorthy, J. Nucl. Mater. 144 (1987) 94.
[23] A.M. Azad, O.M. Sreedharan, J.B. Gnanamoorthy, J. Nucl. Mater. 151 (1988) 293.
[24] J.K.L. Lai, Mater. Sci. Eng. 61 (1983) 101.
[25] S. Rajendran Pillai, H.S. Khatak, J.B. Gnanamoorthy, Mater. Trans. JIM 39 (1998) 370.